

R. Desmorat

LMT (ENS Cachan / CNRS / U. Paris Saclay)

A. du Tertre, P. Gaborit

(Snecma)

E-mail: desmorat@lmt.ens-cachan.fr

DOI : 10.12762/2015.AL09-05

# Multiaxial Haigh Diagrams from Incremental Two Scale Damage Analysis

In High Cycle Fatigue, plasticity and damage are localized at a microscale, a scale smaller than the Representative Volume Element (RVE) scale of continuum mechanics. An incremental two-scale damage model has been built on this basis by Lemaitre et al, and has been mainly applied to alternated loading with no plasticity at the RVE scale. A modified Eshelby-Kröner scale transition law is derived here, taking into account RVE mesoscale plasticity and also microscale plasticity and damage. The ability of the corresponding two-scale damage model to deal with multiaxiality in a wide range of load ratios (from -1 to 0.9) is then focused on.

The crack initiation conditions for axisymmetric notched specimens loaded at different mean stresses are studied on the basis of several fatigue tests on TA6V specimens at a low temperature. Both the notch first loading pre-plastication and the biaxial stress state are naturally taken into account by the incremental analysis. Two multiaxial Haigh diagrams are finally drawn for TA6V at a low temperature. Their main features, such as a horizontal asymptote, are highlighted. A piecewise linear extension for a stronger mean stress effect is finally given within the two-scale damage framework considered.

## Introduction

High fatigue is often addressed in terms of stress amplitude, i.e., with laws directly relating the stress amplitude to the number of cycles to failure or to crack initiation [2, 49, 1, 39, 28]. The mean stress effect is then simply represented by the introduction into the previous law, as a parameter, of the stress ratio  $R = \sigma_{min}/\sigma_{Max}$  (minimum stress divided by the maximum stress over a cycle). The difficulty is then to extend such a modeling to 3D cases and to non-cyclic loading conditions [60, 7, 13, 34, 14, 55, 56, 53, 52].

On the other hand, Continuum Damage Mechanics, naturally a 3D model, can also be used for fatigue [40, 41, 42, 8, 10, 54, 25, 31, 48, 57, 61, 24, 18, 51, 11, 29, 23, 47]. The cyclic relationships are obtained first from the time integration over one cycle of the damage and the constitutive laws, and second from the integration over the entire loading [43]. The introduction of the stress ratio is then not natural and may become a difficult task [46, 3]. One possibility is to model the microdefect or microcrack closure effect (also called quasi-unilateral condition, [36, 9, 21]) and its coupling with damage growth [32, 22]. With this in mind and with the additional fact that High Cycle Fatigue (HCF) corresponds most often to fatigue in the elastic regime, an incremental two scale damage model has been proposed with good fatigue capabilities [44, 45, 17, 38, 26]. Such a

model is extended in this work, in order to recover the mean stress effect obtained in simple but nevertheless representative structures, namely in axisymmetric notched specimens made of a TA6V titanium alloy. The tests have been performed at a low temperature by Snecma, with the support of CNES, within the framework of rocket engine applications.

These specimens have been chosen to represent real loading conditions, i.e., multiaxial conditions with stress triaxialities greater than that encountered under tension and with localized yielding. In order to characterize the model response over the entire stress ratio range from  $R = -1$  to  $R = 0.9$ , TA6V notched specimens with different stress concentration factors  $K_T = 1.5, 2.5$  and  $3.5$  have been tested at different nominal stress – or load – ratios. Axisymmetric notched specimens are found to be very useful to test the HCF behavior of a material submitted to bi-axial stresses at a given – and especially at a high – stress ratio  $R$ . It is indeed quite difficult to "explore" the upper stress ratio domain with classical uniaxial (smooth) specimens, since most of the time, for high numbers of cycles to rupture (i.e., over  $10^6$ ), the mean stress required to obtain  $R > 0.6$  is so high that the yield stress, or even the ultimate stress, are rapidly reached. On the contrary, axisymmetric notched specimens encounter small scale yielding and allow local yielding to be obtained in a biaxial state of stress (the longitudinal and hoop stresses in the notch can represent 70% and 30%

of the stress tensor trace respectively). Once plastified, they allow the material fatigue response to be tested in a simple manner at high stress ratios  $R$ . They can be considered as representative of industrial cases encountered in certain engine components submitted to high static loads and to high frequency alternate loads.

Multiaxial Haigh diagrams are constructed in this work, using a two-scale damage analysis of such tests.

## Two-scale damage model

A two-scale damage model has been built [44, 45, 17, 20, 58] considering that High Cycle Fatigue, either thermally or mechanically activated, occurs for an elastic regime at the RVE scale, the mesoscale of continuum mechanics. It accounts for micro-plasticity and micro-damage at the defect scale (or microscale). The model is phenomenological, describing micro-plasticity with classical 3D Von Mises plasticity equations and describing micro-damage by the Lemaitre damage evolution law  $\dot{D} = (Y/S)^s \dot{p}$  [43, 42] of damage governed by the accumulated plastic strain rate  $\dot{p}$  and enhanced by the strain energy density (with  $Y$  denoting the thermodynamic force associated with the damage variable  $D$ ). Parameters  $S$  and  $s$  are material and temperature dependent. A scale transition law, such as the Eshelby-Kröner localization law, links both the mesoscopic and microscopic scales.

## Incremental two-scale analysis

The general principles for building an initial two-scale damage model for complex fatigue applications are as follows (figure 1). Only isothermal conditions are considered in this work (for the anisothermal case, refer to [21]).

- At the mesoscale, the scale of the RVE of continuum mechanics, the behavior is considered as elastic, the material yield stress  $\sigma_y$ , usually not being reached in HCF.

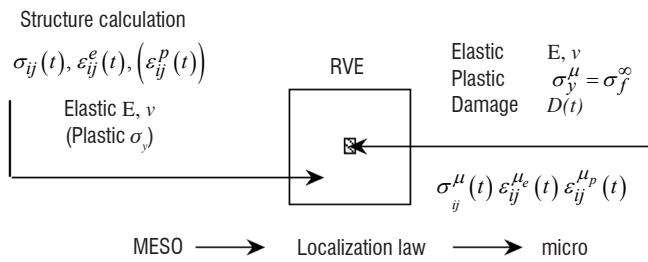


Figure 1 - Micro-element embedded in an elastic Representative Volume Element

- The microscale is the defect scale, with defects conceptually gathered as a weak inclusion embedded in previous RVE. The behavior considered for the microscale is (thermo-)elasto-plasticity coupled with damage, the weakness of the inclusion being represented by a yield stress at the microscale  $\sigma_y^\mu < \sigma_y$  considered equal to the asymptotic fatigue limit of the material  $\sigma_f^\infty$ .

At the mesoscale, the stresses are denoted by  $\sigma$  and the total, elastic and plastic strains are denoted by  $\epsilon$ ,  $\epsilon^e$ ,  $\epsilon^p$ . These are known from an elasto-plastic Finite Element computation. The values at the microscale have an upper-script  $\mu$ , except for the damage variable  $D = D^\mu$  at the microscale, which has no upper-script.

## Scale transition law

In earlier developments within the two-scale damage framework of Lemaitre et al, plasticity and damage were assumed to occur at the microscale only, thus setting  $\epsilon^{\mu p} \neq 0$ ,  $D = D^\mu \geq 0$  but also setting a zero value for the plastic strains at the mesoscale ( $\epsilon^p = 0$ ). In the notched specimen fatigue case considered, the yield stress will be reached at some stress concentration points and plasticity will occur, localized, but nevertheless present at the mesoscale (i.e., present in Finite Element computations of the notched specimens).

The two-scale damage model must be extended, in order to take into account non-zero plastic strains  $\epsilon^p$ , either constant or evolving ( $\epsilon^p(t)$ ) at each time step of an incremental fatigue analysis. A (quite) simple way to proceed is to extend the Eshelby-Kröner scale transition law of a spherical inclusion embedded in an infinite elastic isotropic matrix to our case. In the initial problem [27, 35], the inclusion has the same elastic properties  $\mathbb{E}$  as the matrix and is subject to free strains  $\epsilon_F$ ; the matrix is subjected to a far field strain  $\epsilon$  (or stress  $\sigma$ ).

The strain in the inclusion is then the sum of the far field strain and of an additional strain due to the inclusion free strains and the matrix elasticity (case (a) in figure 2),

$$\epsilon^\mu = \epsilon + \mathbb{S} : \epsilon_F \quad (1)$$

Which is equivalent to

$$\sigma^\mu = \sigma + \mathbb{E} : (\mathbb{S} - \mathbb{I}) : \epsilon_F \quad (2)$$

where  $\mathbb{I}$  is a fourth order identity tensor and where  $\mathbb{S}$  is an isotropic Eshelby tensor such that

$$\mathbb{S} : \mathbf{1} = \alpha \mathbf{1} \quad \alpha = \frac{1+\nu}{3(1-\nu)} \quad (3)$$

for a second order identity tensor  $\mathbf{1}$  and

$$\mathbb{S} : \mathbf{T}' = \beta \mathbf{T}' \quad \beta = \frac{2}{15} \frac{4-5\nu}{1-\nu} \quad (4)$$

for any deviatoric tensor  $\mathbf{T}'$ . By setting  $\epsilon_F$  equal to the micro-plastic strain  $\epsilon^{\mu p}$ , the localization law for an undamaged inclusion used so far [14, 45] is obtained

$$\epsilon^\mu = \epsilon + \beta \epsilon^{\mu p} \quad \text{or} \quad \sigma^\mu = \sigma - 2G(1-\beta) \epsilon^{\mu p} \quad (5)$$

where  $G$  is the shear modulus.

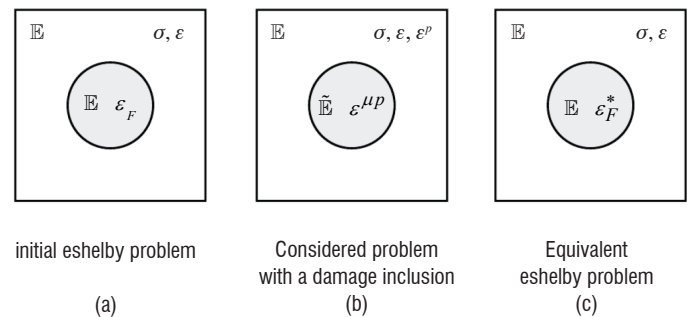


Figure 2 - a) Initial Eshelby problem of an inclusion with free strain  $\epsilon_F$ , b) Considered problem with matrix plasticity and damaged inclusion, c) Problem making both cases a) and b) equivalent, due to an adequate choice of the free strain  $\epsilon_F^*$ .

The problem considered in this work is slightly different, given that the elastic properties of the inclusion  $\tilde{\mathbb{E}} = \mathbb{E}(1-D)$  are affected by the damage  $D$  and given that the matrix withstands (mesoscopic) plastic strains  $\varepsilon^p$  (case (b) of figure 2). It is possible to derive the corresponding localization law from previous Eshelby analysis. Due to the elastic mismatch between both scales, the inclusion must be conceptually changed into an equivalent inclusion with the same total strains and stresses, but with undamaged elasticity (case (c) in figure 2, [30]). In order to do this, an equivalent free strain  $\varepsilon_F^*$  is derived, in which the damage effect is embedded, so that for  $\varepsilon_F^*$  classical expressions (1)-(2) the following is enforced

$$\begin{cases} \sigma^\mu = \tilde{\mathbb{E}} : (\varepsilon^\mu - \varepsilon^{\mu p}) \\ \sigma = \mathbb{E} : (\varepsilon - \varepsilon^p) \\ \varepsilon^\mu = \varepsilon + \mathbb{S} : \varepsilon_F^* \\ \sigma^\mu = \sigma + \mathbb{E} : (\mathbb{S} - \mathbb{I}) : \varepsilon_F^* \end{cases} \quad (6)$$

This therefore defines  $\varepsilon_F^*$ ,

$$\varepsilon_F^* = \left[ \mathbb{E} - (\mathbb{E} - \tilde{\mathbb{E}}) : \mathbb{S} \right]^{-1} : \left[ (\mathbb{E} - \tilde{\mathbb{E}}) : \varepsilon + \tilde{\mathbb{E}} : \varepsilon^{\mu p} - \mathbb{E} : \varepsilon^p \right] \quad (7)$$

The equivalent strain  $\varepsilon_F^*$  replaces  $\varepsilon_F$  in equation (1) so that, after some mathematical arrangements and bearing in mind the fact that a plastic strain tensor is a deviatoric tensor, the modified Eshelby-Kröner scale transition law coupled with damage is obtained:

$$\varepsilon^\mu = \frac{1}{1-\beta D} \left[ \varepsilon + \frac{(\alpha-\beta)D}{3(1-\alpha D)} \text{tr} \varepsilon \mathbf{1} + \beta \left( (1-D) \varepsilon^{\mu p} - \varepsilon^p \right) \right] \quad (8)$$

where  $\alpha$  and  $\beta$  are the previous Eshelby parameters. For an undamaged inclusion ( $D=0$ ) in an elasto-plastic matrix, the previous law is simplified, as expected, to  $\varepsilon^\mu = \varepsilon + \beta \left( \varepsilon^{\mu p} - \varepsilon^p \right)$ .

### Plasticity and damage at the microscale

The history of the stresses  $\sigma(t)$ , strains  $\varepsilon(t)$  and plastic strains  $\varepsilon^p(t)$  at the RVE mesoscale is assumed to be known from an elasto-plastic (incremental) finite element calculation. The scale transition is made using equation (8), which must be solved altogether with microscale constitutive equations (still incremental).

A law of elasto-plasticity coupled with damage is considered at the microscale. The elasticity law is then written as (recall that the  $\mu$ -upper-script stands for "variable at the microscale"):

$$\varepsilon^{\mu e} = \frac{1+\nu}{E} \tilde{\sigma}^\mu - \frac{\nu}{E} \text{tr} \tilde{\sigma}^\mu \mathbf{1} \quad \tilde{\sigma}^\mu = \frac{\sigma^\mu}{1-D} \quad (9)$$

In the yield criterion, the hardening  $\mathbf{X}^\mu$  is kinematic, linear, and the yield stress is the asymptotic fatigue limit of the material, denoted by  $\sigma_f^\infty$ ,

$$f^\mu = (\tilde{\sigma}^\mu - \mathbf{X}^\mu)_{eq} - \sigma_f^\infty \quad (10)$$

where  $(\cdot)_{eq}$  is the Von Mises norm and where  $\tilde{\sigma}^\mu = \sigma^\mu / (1-D)$  is the effective stress and  $f^\mu < 0 \rightarrow$  elasticity. This ensures that micro-plasticity, and therefore damage and failure, occurs for stresses ranging between the fatigue limit  $\sigma_f^\infty$  and the RVE yield stress  $\sigma_y$ .

The set of constitutive equations at the microscale is thus:

$$\begin{cases} \varepsilon^\mu = \varepsilon^{\mu e} + \varepsilon^{\mu p} \\ \varepsilon^{\mu e} = \frac{1+\nu}{E} \tilde{\sigma}^\mu - \frac{\nu}{E} \text{tr} \tilde{\sigma}^\mu \mathbf{1} \\ \dot{\varepsilon}^{\mu p} = \frac{3}{2} \frac{\tilde{\sigma}^{\mu D} - \mathbf{X}^\mu}{(\tilde{\sigma}^\mu - \mathbf{X}^\mu)_{eq}} \dot{p}^\mu = \dot{p}^\mu \mathbf{n} \\ \dot{\mathbf{X}}^\mu = \frac{2}{3} C_y (1-D) \dot{\varepsilon}^{\mu p} \\ \dot{D} = \left( \frac{Y^\mu}{S} \right)^s \dot{p}^\mu \\ D = D_c \rightarrow \text{crack initiation} \end{cases} \quad (11)$$

with the plastic modulus  $C_y$ , the damage strength  $S$ , the damage exponent  $s$  and the critical damage  $D_c$  as material parameters. The damage growth is smaller in compression than in tension, due to the consideration of the micro-defect closure parameter  $h$  within the strain energy release rate  $Y^\mu$ ,

$$Y^\mu = \frac{1+\nu}{2E} \left[ \frac{\langle \sigma^\mu \rangle^+ : \langle \sigma^\mu \rangle^+}{(1-D)^2} + h \frac{\langle \sigma^\mu \rangle^- : \langle \sigma^\mu \rangle^-}{(1-hD)^2} \right] - \frac{\nu}{2E} \left[ \frac{\langle \text{tr} \sigma^\mu \rangle_+^2}{(1-D)^2} + h \frac{\langle \text{tr} \sigma^\mu \rangle_-^2}{(1-hD)^2} \right] \quad (12)$$

since  $0 < h < 1$  and usually for metals  $h \approx 0.2$  [43], and where  $\langle \cdot \rangle_+$ ,  $\langle \cdot \rangle_-$  stand for the positive and negative parts of a scalar and  $\langle \cdot \rangle^+$ ,  $\langle \cdot \rangle^-$  for the positive and negative parts of a tensor (in terms of principal values). Note that equation (12) is simplified to

$$Y_{tens}^\mu = (\sigma^\mu)^2 / 2E(1-D)^2 \quad \text{for tension at the microscale and in}$$

$$Y_{comp}^\mu = h(\sigma^\mu)^2 / 2E(1-hD)^2 \quad \text{for compression at the microscale,}$$

so that the damage rate in compression  $\dot{D}_{comp} = (Y_{comp}^\mu / S)^s \dot{p}^\mu$  is much lower, for a small  $h$ , than the damage rate in tension  $\dot{D}_{tens} = (Y_{tens}^\mu / S)^s \dot{p}^\mu$ .

In previous constitutive equations,  $p^\mu = \int_0^t (\frac{2}{3} \dot{\varepsilon}^{\mu p} : \dot{\varepsilon}^{\mu p})^{1/2} dt$  is the

accumulated plastic strain at the micro-scale and no damage threshold is considered (for loading dependent thresholds, refer to [45, 46]). The plastic multiplier  $\dot{\lambda} = \dot{p}^\mu (1-D)$  is determined from the consistency condition  $f^\mu = 0$  and  $\dot{f}^\mu = 0$ .

The internal variables  $\varepsilon^{\mu p}$ ,  $p^\mu$  and  $D^\mu = D$  are often considered to be equal to zero at  $t=0$ . A pre-hardening or pre-damage correspond to non-vanishing initial values  $\varepsilon^{p0}$ ,  $p_0$ ,  $D_0$  for the time integration of the differential equations (11): pre-hardening is naturally accounted for in a rate form modeling [5]. Note also that the localization law takes into account the plastic strain evolution  $\varepsilon^p(t)$  at the RVE scale. This means that the pre-plasticification stage of the structures before undergoing elastic fatigue is taken into account by means of the  $\varepsilon^p$ -term of the scale transition law (8). Further study of notched specimens loaded at high mean stresses uses this feature (§ "Fatigue of axisymmetric notched specimens").

## Numerical implementation

With regard to the numerical implementation, a post-processing approach is proposed. The strain and plastic strain histories at the mesoscale are assumed to be known from a reference Finite Element elastic or elasto-plastic computation. The micro-plasticity and damage are obtained by the time integration, step by step, of the incremental constitutive equations. At each time step  $t_{n+1}$  and for a known strain increment at the mesoscale  $\Delta\varepsilon = \varepsilon_{n+1} - \varepsilon_n$ , the numerical scheme must calculate, by time integration of the constitutive equations at the microscale together with the consideration of the localization law, the strain  $\varepsilon_{n+1}^\mu$ , stress  $\sigma_{n+1}^\mu$ , plastic strain  $\varepsilon_{n+1}^{\mu p}$ , accumulated plastic strain  $p_{n+1}^\mu$  and damage  $D_{n+1}$  at microscale. The Euler backward scheme is used to discretize their rate form, as for classical single scale plasticity and damage models. The 3 stages for the numerical resolutions of the two-scale model equations are classically [44, 46, 20]: 1) an elastic prediction at the microscale, taking into account the localization law, 2) a test over the criterion function  $f^\mu$ , and 3) if  $f^\mu$  is found to be positive, a plastic-damage correction (still at the microscale).

### Elastic Prediction

The elastic prediction assumes an elastic behavior at the microscale with constant plastic strain  $\varepsilon_{n+1}^{\mu p} = \varepsilon_n^{\mu p}$ , constant kinematic hardening  $\mathbf{X}_{n+1}^\mu = \mathbf{X}_n^\mu$  and constant damage  $D_{n+1} = D_n$ . The elastic prediction gives a first estimate for the total strain, the elastic strain and the effective stress at the microscale at time  $t_{n+1}$ ,

$$\varepsilon^\mu = \frac{1}{1-\beta D_n} \left\{ \varepsilon_{n+1} + \frac{(\alpha-\beta)D_n}{3(1-\alpha D_n)} \text{tr} \varepsilon_{n+1} \mathbf{1} + \beta \left[ (1-D_n) \varepsilon_n^{\mu p} - \varepsilon_{n+1}^p \right] \right\} \quad (13)$$

$$\varepsilon^{\mu e} = \varepsilon^\mu - \varepsilon_n^{\mu p}$$

$$\tilde{\sigma}^\mu = \mathbb{E} : \varepsilon^{\mu e}$$

$$\sigma^\mu = (1-D_n) \tilde{\sigma}^\mu$$

### Plastic-damage correction

The previous elastic prediction gives the estimate  $\tilde{\sigma}$  of the effective stress  $\tilde{\sigma}_{n+1}$  at time  $t_{n+1}$ , with unchanged kinematic hardening  $\mathbf{X} = \mathbf{X}_n$ , and allows the yield criterion to be calculated. If the condition  $f_{n+1}^\mu \leq 0$  is fulfilled, the calculation is over and  $\varepsilon_{n+1}^{\mu p} = \varepsilon_n^{\mu p}$ ,  $\mathbf{X}_{n+1}^\mu = \mathbf{X}_n^\mu$ ,  $D_{n+1} = D_n$  is set. If not, this elastic solution is corrected by ensuring the consistency condition  $f_{n+1}^\mu = 0$ . The Euler Backward scheme is used for all variables except damage:  $D = D_n$  is considered over a time step  $\Delta t = t_{n+1} - t_n$  in the strain localization law and in plasticity equations coupled with damage. This is of course not a limitation at all in fatigue, since over an entire cycle – made up of many time steps – the damage increment usually does not exceed  $D_c / N_R < 10^{-3}$  where  $D_c \leq 1$  is the critical damage and  $N_R$  is the number of cycles to crack initiation.

Assuming then that the damage does not increase much over a time step, the set of nonlinear equations (11) must be solved, including the localization law,

$$\Delta \varepsilon^{\mu e} + \frac{1-\beta}{1-\beta D_n} \Delta \varepsilon^{\mu e} - \frac{1}{1-\beta D_n} \Delta \varepsilon + \frac{\beta}{1-\beta D_n} \Delta \varepsilon^p - \frac{(\alpha-\beta)D_n}{(1-\beta D_n)(1-\alpha D_n)} \text{tr} \Delta \varepsilon \mathbf{1} = 0 \quad (14)$$

and the yield condition  $f^\mu = 0$  at time  $t_{n+1}$

$$f_{n+1}^\mu = (\tilde{\sigma}_{n+1}^\mu - \mathbf{X}_{n+1}^\mu)_{eq} - \sigma_f^\infty = 0 \quad (15)$$

Equations (14)-(15) are combined with the normality rule for plastic strain and with the evolution law for kinematic hardening, discretized as  $\Delta \varepsilon^{\mu p} = \frac{3}{2} \frac{\tilde{\sigma}_{n+1}^{\mu D} - \mathbf{X}_{n+1}^\mu}{(\tilde{\sigma}_{n+1}^\mu - \mathbf{X}_{n+1}^\mu)_{eq}} \Delta p^\mu = \frac{3}{2} \frac{\mathbf{s}_{n+1}^{\mu D}}{(\tilde{\sigma}_{n+1}^\mu)_{eq}} \Delta p^\mu$  and  $\Delta \mathbf{X}^\mu = \frac{2}{3} C_y (1-D_n) \Delta \varepsilon^{\mu p}$ . These equations can of course be

solved using the Newton iterative method, but must be rewritten in the following form,

$$\begin{cases} \frac{\mathbf{s}_{n+1}^\mu}{E} + \Gamma \frac{\mathbf{s}_{n+1}^{\mu D}}{(\mathbf{s}_{n+1}^\mu)_{eq}} \Delta p^\mu + \mathbf{Q}_s = 0 \\ (\mathbf{s}_{n+1}^\mu)_{eq} - \sigma_f^\infty = 0 \end{cases} \quad (16)$$

a function of the unknown accumulated plastic strain increment  $\Delta p^\mu$  and of the unknown variable  $\mathbf{s}_{n+1}^\mu = \tilde{\sigma}_{n+1}^\mu - \mathbf{X}_{n+1}^\mu$  allows a closed-form solution to be obtained explicitly. The following is set in Equations (16) (details can be found in [20]):

$$\mathbf{Q}_s = -\frac{\tilde{\sigma}_n^\mu - \mathbf{X}_n^\mu}{E} - \frac{1}{E(1-\beta D_n)} \times \left[ \mathbb{E} : \Delta \varepsilon + K \frac{(\alpha-\beta)D_n}{1-\alpha D_n} \text{tr} \Delta \varepsilon \mathbf{1} - 2G\beta \Delta \varepsilon^p \right] \quad (17)$$

$$\Gamma = \frac{1}{E} \left( 3G \frac{1-\beta}{1-\beta D_n} + C_y (1-D_n) \right)$$

where  $G = E/2(1+\nu)$  and  $K = E/3(1-2\nu)$  are the shear and bulk moduli.

The exact solution of the set of equations (16) for the plastic-damage correction is:

$$s_{H\ n+1}^\mu = -EQ_{sH}$$

$$\Delta p^\mu = \frac{1}{\Gamma} \left( Q_{seq} - \frac{\sigma_f^\infty}{E} \right)$$

$$(\mathbf{s}_{n+1}^\mu)' = -\frac{E\mathbf{Q}_s'}{1 + \frac{\Gamma E}{\sigma_f^\infty} \Delta p^\mu} \quad (18)$$

$$\mathbf{s}_{n+1}^\mu = (\mathbf{s}_{n+1}^\mu)' + s_{H\ n+1}^\mu \mathbf{1}$$

where  $Q_{seq} = \sqrt{\frac{3}{2} \mathbf{Q}_s' : \mathbf{Q}_s'}$  is the Von Mises norm of  $\mathbf{Q}_s$ ,  $Q_{sH} = \frac{1}{3} \text{tr} \mathbf{Q}_s$  is its hydrostatic part and  $\mathbf{Q}_s' = \mathbf{Q}_s - Q_{sH} \mathbf{1}$  is its deviatoric part.

The proposed scheme is implicit but does require iterations.

### Variable updating

Once the previous plastic-damage correction has been made, all of the variables at the microscale are updated as follows:

- normal to the yield surface:  $\mathbf{m}^\mu = \frac{3}{2} \frac{\mathbf{s}_{n+1}^{\mu D}}{\sigma_f^\infty}$
- plastic strain:  $\varepsilon_{n+1}^{\mu p} = \varepsilon_n^{\mu p} + \mathbf{m}^\mu \Delta p^\mu$
- kinematic hardening:  $\mathbf{X}_{n+1}^\mu = \frac{2}{3} C_y (1 - D_n) \Delta \varepsilon_{n+1}^{\mu p} + \mathbf{X}_n^\mu$
- effective stress:  $\tilde{\sigma}_{n+1}^\mu = \mathbf{s}_{n+1}^\mu + \mathbf{X}_{n+1}^\mu$
- damage:

$$D_{n+1} = D_n + \left( \frac{Y_{n+1}^\mu}{S} \right)^s \Delta p^\mu \quad \text{with}$$

$$Y_{n+1}^\mu = \frac{1+\nu}{2E} [\langle \tilde{\sigma}_{n+1}^\mu \rangle^+ : \langle \tilde{\sigma}_{n+1}^\mu \rangle^+ + h \left( \frac{1-D_n}{1-hD_n} \right)^2 \langle \tilde{\sigma}_{n+1}^\mu \rangle^- : \langle \tilde{\sigma}_{n+1}^\mu \rangle^-] - \frac{\nu}{2E} [\langle \text{tr} \tilde{\sigma}_{n+1}^\mu \rangle_+^2 + h \left( \frac{1-D_n}{1-hD_n} \right)^2 \langle \text{tr} \tilde{\sigma}_{n+1}^\mu \rangle_-^2]$$

- stress tensor :  $\sigma_{n+1}^\mu = (1 - D_{n+1}) \tilde{\sigma}_{n+1}^\mu$   
and the calculation can then be started at time  $t_{n+2}$

### DAMAGE EAS post-processor for multiaxial fatigue

The DAMAGE\_EAS post-processor solves the two-scale damage model constitutive equations and allows the micro-plasticity and damage history to be determined for complex loading. For a given material parameter file and for a given loading sequence (made up of the repetition by blocks of complex cycles defined at the RVE mesoscale), the post-processor calculates the damage history  $D(t)$  and the time to crack initiation, i.e., the time for  $D$  to reach the critical damage  $D_c$ . The inputs (mesostrains, total and plastic) come from a Finite Element reference computation and are thus at one or several user chosen structure Gauss points. Given that the maximum number of increments used to describe a cycle is large (actually 5000), the program allows quasi random fatigue calculations. The post-processor DAMAGE\_EAS has a graphical interface with material parameter identification and result plotting capabilities [19].

The inputs are thus a material file and a loading file. The outputs of any calculation are:

- the number of cycles to crack initiation for the case considered;
- a standard result file made up of 50 lines with the values (the histories) versus the number of cycles of the accumulated plastic strain and of the damage at the microscale;
- optional (large) files for complete results at the mesoscale and microscale (stresses, strains and plastic strain components versus time).

### Fast identification procedure

The purpose of this work is to study the ability of the model to handle notched structure fatigue, when the material parameters are first identified on tensile uniaxial (or "smooth") testing specimens. For the parameter identification, the following is proposed.

Stage 1. The mesoscale parameters (Young modulus  $E$ , Poisson ratio  $\nu$ , yield stress  $\sigma_y$ , plastic modulus  $C_y$ ) are identified at each temperature on the monotonic tensile curve.

Stage 2. The asymptotic fatigue limit  $\sigma_f^\infty$  is guessed from an experimental Wöhler curve as the horizontal "asymptote" at a very high number of cycles to rupture (at least  $N_R > 10^7$ ),

$$\frac{\Delta \sigma}{2} \rightarrow \frac{(\Delta \sigma)^\infty}{2} = \sigma_f^\infty \Rightarrow N_R \rightarrow \infty$$

For a non-symmetric fatigue loading (and in this model because of the Von Mises yield criterion at the microscale), the asymptote in terms of

the stress amplitude  $\frac{(\Delta \sigma)^\infty}{2} = \sigma_f^\infty$  is independent from the load ratio

$R = \sigma_{min} / \sigma_{Max}$ . In terms of maximum stress, the corresponding asymptote is  $\sigma_{Max}^\infty = 2\sigma_f^\infty / (1-R)$  – it is still due to

$$\frac{(\Delta \sigma)^\infty}{2} = \frac{\sigma_{Max}}{2} (1-R) = \sigma_f^\infty \quad \text{– and is dependent on } R.$$

If the  $\sigma_{Max}$  vs.  $N_R$  diagram is used, the guessed horizontal asymptote  $\sigma_{Max}^\infty$  at a given load ratio  $R$  thus allows the – material parameter – fatigue limit  $\sigma_f^\infty$  to be identified as:

$$\sigma_f^\infty = \frac{1}{2} (1-R) \sigma_{Max}^\infty \quad (19)$$

Stage 3. The parameters  $h$  and  $D_c$  are considered to be equal to the default constant values for metals,  $h = 0.2$ ,  $D_c = 0.3$  [43].

Stage 4. The damage parameters  $S$  and  $s$  are pre-identified from a non-linear curve fitting in Wöhler diagram (figure 3) using an approximate closed-form expression for  $N_R$  (under the assumption  $h = 1$  of a no micro-defect closure effect). This allows a first estimate of the damage parameters  $S$  and  $s$  to be easily determined. For a cyclically varying stress of  $\Delta \sigma = \sigma_{Max} - \sigma_{min}$  between  $\sigma_{min}$  and  $\sigma_{Max}$ , the following closed form expression for the number of cycles to rupture is used [15, 16], here with no damage threshold,

$$N_R \approx \frac{(2ES)^s \mathcal{G} D_c}{\sigma_f^{\infty 2s} [\Delta \sigma - 2\sigma_f^\infty] [R_{vmin}^s + R_{vMax}^s]} \quad (20)$$

$$\mathcal{G} = 3G(1-\beta) + C_y(1-D) \approx 3G(1-\beta),$$

$$R_{vmin} = \frac{2}{3}(1+\nu) + \frac{1}{3}(1-2\nu) \left[ \frac{\sigma_{min}}{\sigma_f^\infty} \right]^2$$

$$R_{vMax} = \frac{2}{3}(1+\nu) + \frac{1}{3}(1-2\nu) \left[ \frac{\sigma_{Max}}{\sigma_f^\infty} \right]^2$$

where  $G$  is the shear modulus.

Stage 5. At this final identification stage, the values for all parameters are kept identical, except for the damage strength  $S$ ;  $h = 0.2$  is set and the parameter  $S$  is re-adjusted by comparison with the reference Wöhler curve. The full set of constitutive equations is solved – numerically this time – instead of using the approximate formula (20).

An illustration of Stages 4 and 5 of the identification procedure is given for a TA6V alloy at a low temperature in figure 3, in which the experimental fatigue curve and the analytic (from equation 20) and computed (DAMAGE\_EAS) model responses are sketched and compared.

The final set of material parameters is only composed of the elasticity parameters  $E$ ,  $\nu \approx 0.3$ , the plastic modulus  $C_y$ , the asymptotic fatigue limit  $\sigma_f^\infty$ , the damage strength  $S$  (in MPa), the damage exponent  $s$ , the micro-defect closure effect parameter  $h = 0.2$  and the critical damage  $D_c = 0.3$ . Let us point out that the identification of parameters  $S$ ,  $s$  and  $\sigma_f^\infty$  is carried out by using a first population of uniaxial (smooth) specimens at  $R = 0.1$  (test results reported as marks in figure 3). Next, the model is evaluated on a second independent population of notched specimens made of the same material, tested at the same temperature, but at higher stress ratios.

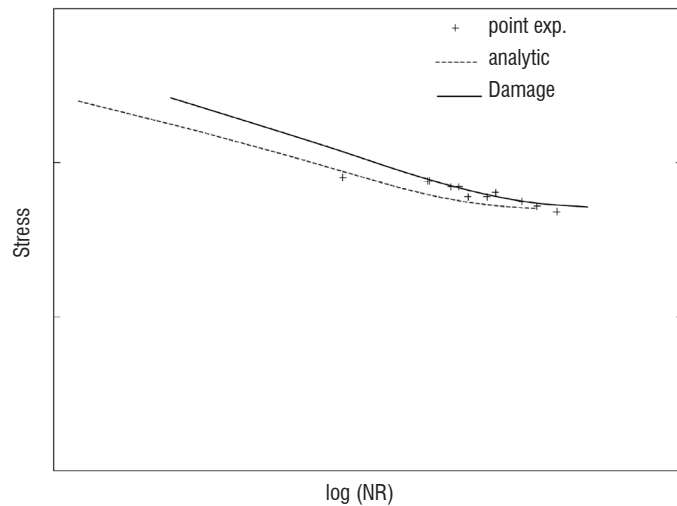


Figure 3 - Illustration of Stages 4 and 5 of the identification procedure on the Wöhler curve for TA6V at a low temperature (marks: experimental, analytical: Eq. (20), DAMAGE: numerical solution by DAMAGE\_EAS of set of equations (8) and (11)).

### Fatigue of axisymmetric notched specimens

Axisymmetric Finite Element computations of 3 notched specimens have been performed with a refined mesh in the notch (figure 4). The three elastic stress concentration factors are  $K_T = 1.5, 2.5$  and  $3.5$ . The specimen height is 60 mm.

Elasto-plastic constitutive equations with linear kinematic hardening are used to model TA6V behavior. The considered stress ratios are positive, the notch plastification only occurs at the first load application. The microscale behavior is represented by the elasto-plasticity coupled with damage constitutive equations (11). The scale transition law is Eq. (8).

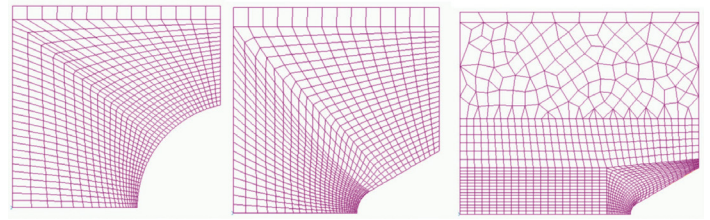


Figure 4 - Details of the meshes in the notch for  $K_T = 1.5$  (left),  $K_T = 2.5$  (middle) and  $K_T = 3.5$  (right).

### Structure computations with pre-plastification

The applied loading is presented in figure 5. It consists in a uniaxial (longitudinal) load varying between a maximum load  $F_{Max}$  and a minimum load  $F_{min}$ . Various maximum loads are considered, corresponding to different numbers of cycles to crack initiation. Various positive load ratios  $R_F = F_{min} / F_{Max}$  are also considered, which are equal to the (applied) far field stress ratio and to the local longitudinal stress ratio  $\sigma_{min} / \sigma_{Max}$  obtained in elastic computations. As mentioned already, plastification takes place in the stress concentration zone during the first load application (a stage therefore called pre-plastification) making the local stress ratio  $R$  obtained in plasticity different from the applied load ratio  $R_F$  (The value of obtained is lower than  $R_F$ ).

An example of a map of accumulated plastic strains in the notch is given in figure 6 for  $F_{min} = 46 \text{ kN}$ ,  $F_{Max} = 52 \text{ kN}$ ,  $R_F = 0.88$ . Simply note that this pre-plastification is naturally taken into account within the two-scale damage model, through the use of the localization law (8) (through the existence of a mesoscopic plastic strain  $\epsilon^p$ ).

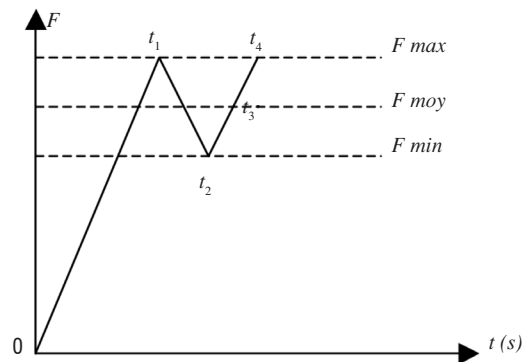


Figure 5 - Applied loading

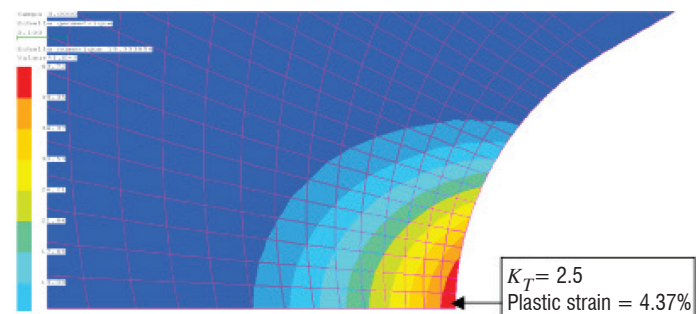


Figure 6 - Maps of plastic strain after pre-plastification for one of the  $K_T = 2.5$  specimens (applied load ratio  $R_F = F_{min} / F_{Max} = 0.88$ , computed stress ratio  $R = \sigma_{min} / \sigma_{Max} = 0.72$ ).

## Number of cycles to rupture from two-scale damage analysis

For the calculations of the numbers of cycles to crack initiation (or for the prediction of the "no crack initiation" events), the total  $\varepsilon$  and plastic  $\varepsilon^p$  strain tensors have been interpolated at the node located at the surface of the notch. These data constitute the input of the DAMAGE EAS post-processor and are entered in the form of an ASCII file. The tensors are extracted from the plasticity computations at time steps  $t_1, t_2, t_3$  and  $t_4$  defined in figure 5. Only the second part of the loading – the part between  $F_{Max}$  and  $F_{min}$  – is repeated. A maximum number of repetitions of this sequence or block must be set when using DAMAGE\_EAS ( $10^7$  in these calculations). The 21 damage post-processings corresponding to 21 tested notched specimens were made in a single (batch) operation taking approximately 45 min on a PC.

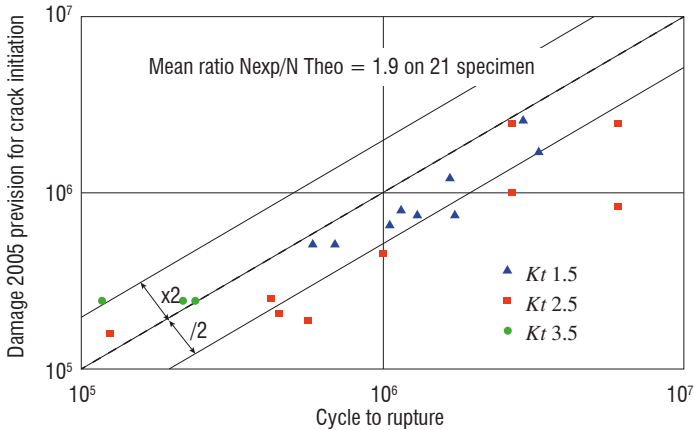


Figure 7 - Comparison between the experimental and predicted lifetimes for axisymmetric notched specimens

Failure is interpreted here as the mesocrack initiation condition, which corresponds to when the damage  $D$  reaches the critical value  $D_c$  (a material parameter here equal to 0.3).

The results obtained show an average ratio Experimental number of cycles to failure  $N_R^{exp}$  / Calculated number of cycles  $N_R^{calc} = N(D = D_c)$  of 1.9 (figure 7). As far as the unbroken specimens at cycles are concerned, the model correctly predicts the non-initiation of a crack in 10 out of 12 cases (83%). The fact that most of the predictions underestimate the experimental fatigue lifetimes seems logical. We must indeed recall that the model only predicts the crack initiation at the RVE mesoscale and does not take into account the cycles necessary to make these small cracks propagate to the final structural failure.

As far as the results obtained here for the TA6V alloy at a low temperature are concerned, the mean factor  $\approx 2$  obtained is quite a good result: this corresponds to the expected performance of a model for its industrial use, when the results are obtained from an independent identification on uniaxial (smooth) fatigue specimens. What is also of utmost importance is the ability of the model to correctly predict the time to crack initiation of a specimen subjected to a high mean stress effect, with more or less plastification (up to 5% here) and for a multiaxial stress state.

## Computed Haigh diagram for TA6V alloy at a low temperature

The classical Haigh diagram corresponds to the curve given, at a given number of cycles to failure, by the stress amplitude

$$\sigma_a = \frac{1}{2}(\sigma_{Max} - \sigma_{min}) \text{ versus the mean stress } \bar{\sigma} = \frac{1}{2}(\sigma_{min} + \sigma_{Max}).$$

First, in order to better characterize the model response over the entire stress ratio range,  $R \in [-1, 0.9]$ , several theoretical times to crack initiation have been calculated using uniaxial strain and plastic strain tensors (i.e., corresponding to uniaxial stress states of smooth specimens) generated for different maximum stresses at a given  $R$ . The corresponding points are reported on the different iso- $R$  lines ( $R = 0.1, 0.5, 0.6, 0.8$  and  $0.9$ , figure 9). Each

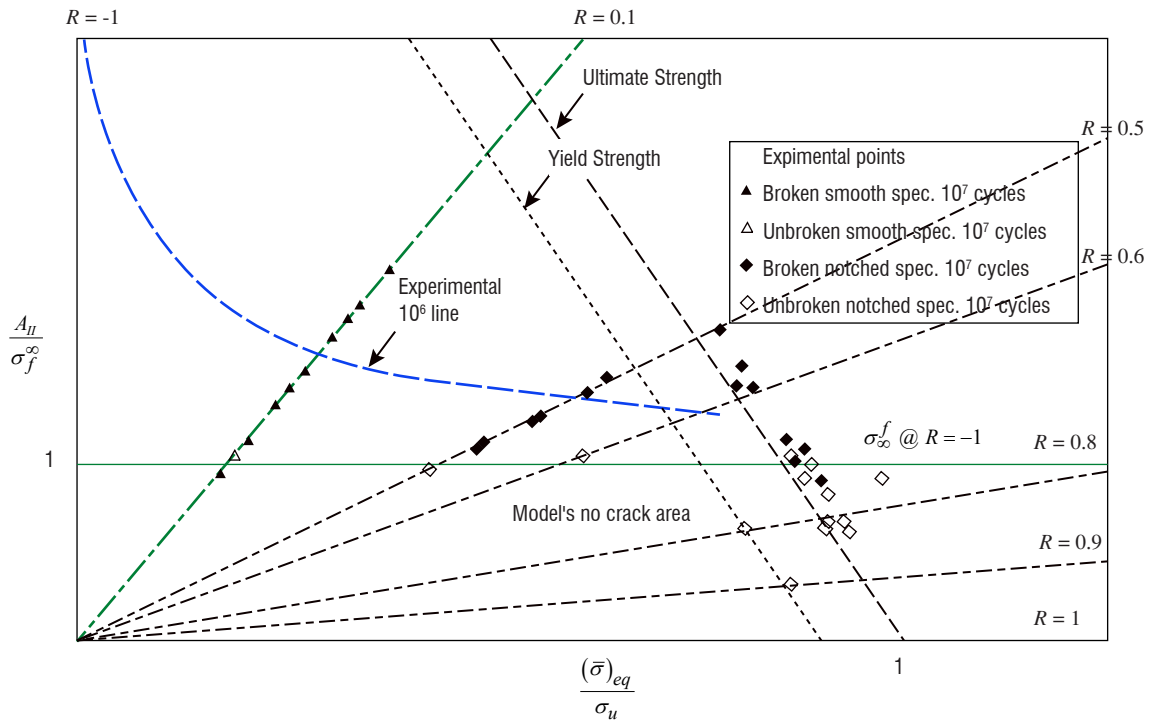


Figure 8 - Experimental multiaxial  $A_{II} / \sigma_f^\infty$  vs.  $(\bar{\sigma})_{eq} / \sigma_u$  Haigh diagram of a TA6V alloy at a low temperature

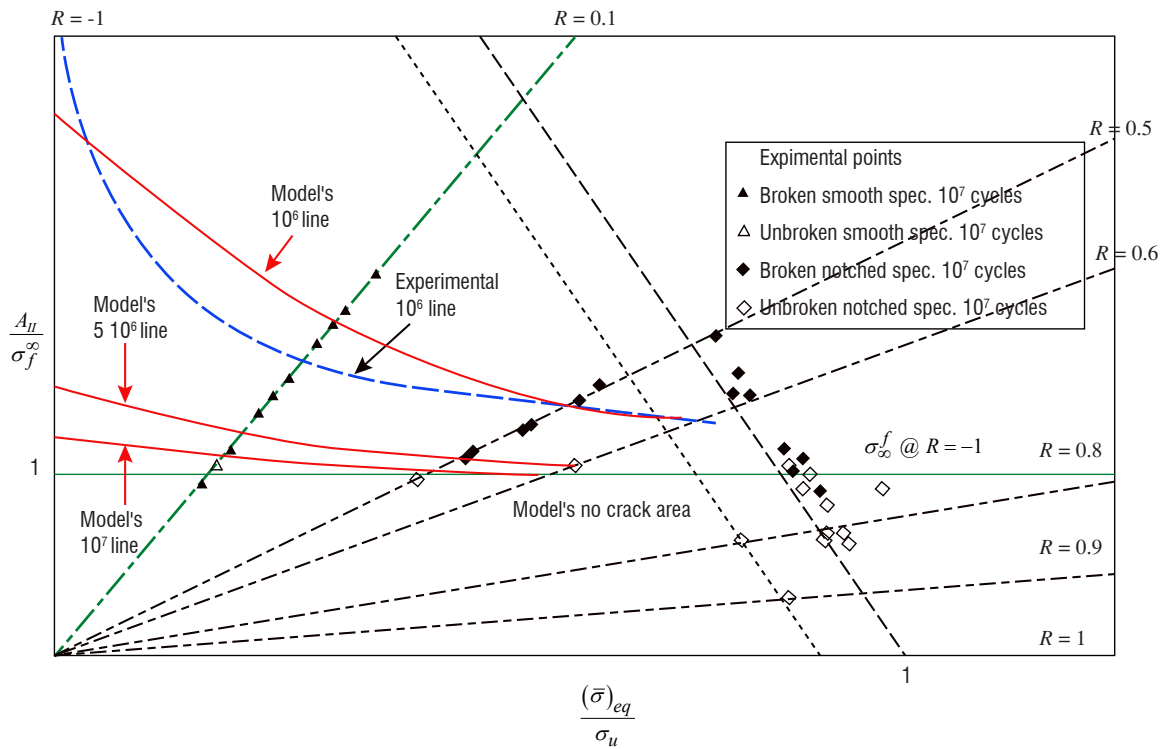


Figure 9 - Multiaxial  $A_{II} / \sigma_f^\infty$  vs.  $(\bar{\sigma})_{eq} / \sigma_u$  Haigh diagram with two-scale damage model iso-lifetime lines

point is associated with a number of cycles to crack initiation calculated by DAMAGE EAS. The maximum stress was systematically chosen above the  $\sigma_f^\infty$ -fatigue limit identified for the material at  $R = -1$  which is, in this two-scale analysis, the limit below which the model does not announce any crack initiation. With such a network of theoretical points associated with their lifetime prediction, it is then possible to plot both the experimental (here at  $N_R = 10^6$  cycles, "Experimental 1E6 line") and the theoretical iso-lifetime curves (using a Box-Cox regression technique). The iso-lifetime curves given by the two-scale damage model for  $10^6$ (1E6),  $5 \cdot 10^6$ (5E6) and  $10^7$ (1E7) cycles are shown in figure 9, each corresponding to a classical Haigh diagram for this TA6V alloy.

#### $A_{II}$ vs. $(\bar{\sigma})_{eq}$ multiaxial Haigh diagram

Both the experimental and computational results have been reported in figures 8 and 9 (by means of the two scale damage analysis). The asymptotic fatigue limit and the ultimate stress are respectively denoted by  $\sigma_f^\infty$  and  $\sigma_u$ . The unbroken specimens after  $10^7$  cycles are represented by white marks, whereas the broken ones are represented by plain black marks. The smooth specimens ( $R = 0.1$ ) are represented by triangular marks. The notched specimens are represented by diamonds marks. For these, the stress state is 3D so a first multiaxial Haigh diagram can be plotted by replacing the uniaxial stress amplitude (vertical axis) by the octahedral shear  $A_{II}$ , the local equivalent alternated stress,

$$\sigma_a = A_{II} = \frac{1}{2} \sqrt{\frac{3}{2} (\sigma'_{Max} - \sigma'_{min}) : (\sigma'_{Max} - \sigma'_{min})} \quad (21)$$

and by replacing the uniaxial mean stress (horizontal axis) by the Von Mises equivalent stress of the mean stress tensor, the mean local stress is

$$(\bar{\sigma})_{eq} = \frac{1}{2} \sqrt{\frac{3}{2} (\sigma'_{Max} + \sigma'_{min}) : (\sigma'_{Max} + \sigma'_{min})} \quad (22)$$

The horizontal line  $A_{II} / \sigma_f^\infty = \sigma_a / \sigma_f^\infty = 1$  or  $A_{II} = \sigma_a = \sigma_f^\infty$  corresponds to the infinite alternated fatigue limit (identified from the § "Fast identification" procedure). It is interesting to notice that, for this TA6V at a low temperature, this limit separates the broken specimens (black marks) from the unbroken ones (white marks) quite well. Note that the model theoretical iso-lifetime curves drawn here are rapidly decreasing in the  $-1$  to  $0.1$ -range. All of the lines converge towards the asymptotic fatigue limit identified at  $R = -1$  (horizontal line  $\sigma_a / \sigma_f^\infty = 1$ ). This line constitutes an asymptote for the iso-lifetime curves when the number of cycles to crack initiation increases. This feature is due to the fact that the equation for the asymptote is  $f'' = 0$  and that in this case a Von Mises plasticity criterion is considered at the microscale.

In order to directly compare the theoretical iso-lifetime curves to their experimental counterparts, a more detailed study can be carried out on the  $N_R = 10^6$  line – which corresponds to the usual Haigh diagram at  $10^6$  cycles – for both the theoretical predictions and the available experimental data. A non-linear data regression allows the experimental  $10^6$ (1E6) iso-life line (dashed line) to be plotted. It is remarkable that the experimental line fits its theoretical counterpart quite well. The global decreasing shape of the  $N_R = 10^6$  computed Haigh diagram is quite similar to that of the experimental one: the two-scale damage model proposes an evolution of the theoretical iso-lifetime curve in good accordance with the experimental  $N_R = 10^6$  line evolution for this TA6V alloy at a low temperature.

Finally, the influence of the local plastification on the local true stress ratio can also be observed. Once the yield stress is reached (straight line "Yield Strength" in figure 8), the local stress ratio computed at the notch tip decreases and the corresponding point leaves its original

iso-R line. All plastified points accumulate along the 45° "Ultimate Strength" straight line. This phenomenon has already been observed [37] and shows the importance of considering the local stress and strain state when drawing Haigh diagrams for notched specimens.

### $A_{II}$ vs. $\text{tr}\bar{\sigma}$ multiaxial Haigh diagram

It is also possible to use another multiaxial extension of the Haigh diagram, the octahedral shear  $\sigma_a = A_{II}$  versus the trace of the mean stress tensor,

$$\text{tr}\bar{\sigma} = \bar{\sigma}_{11} + \bar{\sigma}_{22} + \bar{\sigma}_{33} \quad \text{with} \quad \bar{\sigma} = \frac{1}{2}(\sigma_{min} + \sigma_{Max}) \quad (23)$$

This complementary representation offers the advantage of better taking the stress triaxiality into account (it is consistent with the Sines approach of multiaxial fatigue [59]). The further values of the stress tensor trace are those of the smooth and notched fatigue specimens, computed by Finite Elements.

In figure 10, three different iso-lifetime lines predicted by the two-scale damage model have been plotted: the  $5 \cdot 10^5$  (5E5),  $10^6$  (1E6) and  $5 \cdot 10^6$  (5E6) iso-lifetime lines, with the corresponding experimental points. Several fatigue tests carried out on smooth specimens at  $R = -1$ ,  $R = 0.1$  and  $R = 0.5$  up to  $10^6$  cycles, allow the shape of the  $N_R = 10^6$  cycles line to be confirmed. As mentioned before, the theory and experiments fit quite well.

Figure 11 is the equivalent of figure 9 (with  $(\bar{\sigma})_{eq}$  replaced by  $\text{tr}\bar{\sigma}$ ). The level of local triaxiality and yielding for each test is better apprehended (this information was not clear in figure 9, since all plastified points were aligned).

Let us insist once again on the fact that the observations made here only concern locally plastified specimens. It would not have been possible to explore such high stress ratio values and such high plastification levels in the High Cycle Fatigue with uniaxial smooth specimens.

### Stronger asymptotic mean stress effect

The mean stress obtained previously in the mean stress range considered was in fact not so important, so that it has been modeled through the dissymmetry of damage growth (by means of a low fatigue limit and a micro-crack closure parameter  $h \ll 1$ ). A more general model is possible, still within the kinetic framework of rate form damage modeling, i.e., still with no need for the notion of cycle or for the Rainflow-type counting cycle method.

### Linear mean stress effect

A linear mean stress effect on the fatigue asymptote can be introduced into the two-scale damage model by considering a Drucker-Prager criterion function at the microscale [3, 4], where is a material parameter,

$$\begin{aligned} f^\mu &= (\sigma^\mu - X^\mu)_{eq} + a \text{tr}\sigma^\mu - \sigma_f^\infty \\ &= (\sigma^\mu - X^\mu)_{eq} + 3a\sigma_H - \sigma_f^\infty \end{aligned} \quad (24)$$

i.e., by making the fatigue criterion pressure/first invariant dependent, as proposed by many authors [12, 59, 13, 24, 42, 50] for fatigue. From the Eshelby-Kröner scale transition law (5) – as well as from the scale transition law (8) – and incompressible plasticity,  $\text{tr}\sigma^\mu = \text{tr}\sigma = 3\sigma_H$  is still obtained. The differences here compared with classical works are: (i) the infinite lifetime domain  $f^\mu < 0$  is translated by micro-plasticity, (ii) the current values of the stresses are used (not the maximum or mean values) and the modeling remains incremental. Micro-plasticity and damage are the solution of a kinetic differential equation, so there is no need to define a cycle in order to calculate the time to crack initiation (it is the time at which  $D(t) = D_c$ , the critical damage).

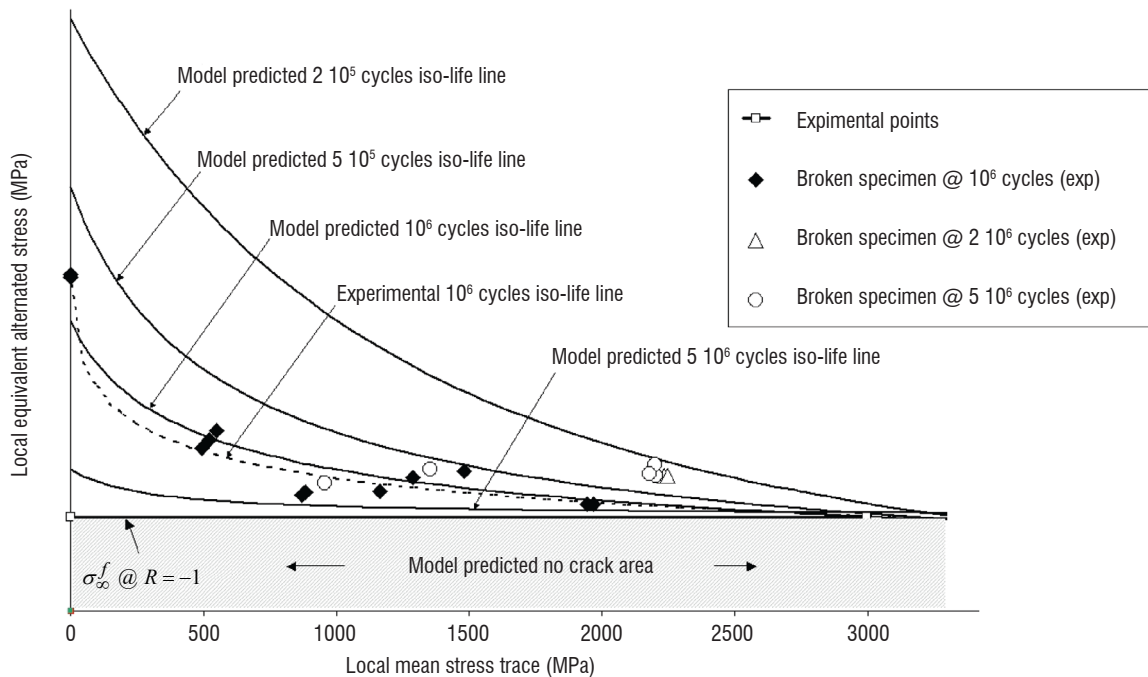


Figure 10 - Partial multiaxial  $A_{II} / \sigma_f^\infty$  vs.  $\text{tr}\bar{\sigma}$  Haigh diagram (TA6V alloy at a low temperature).

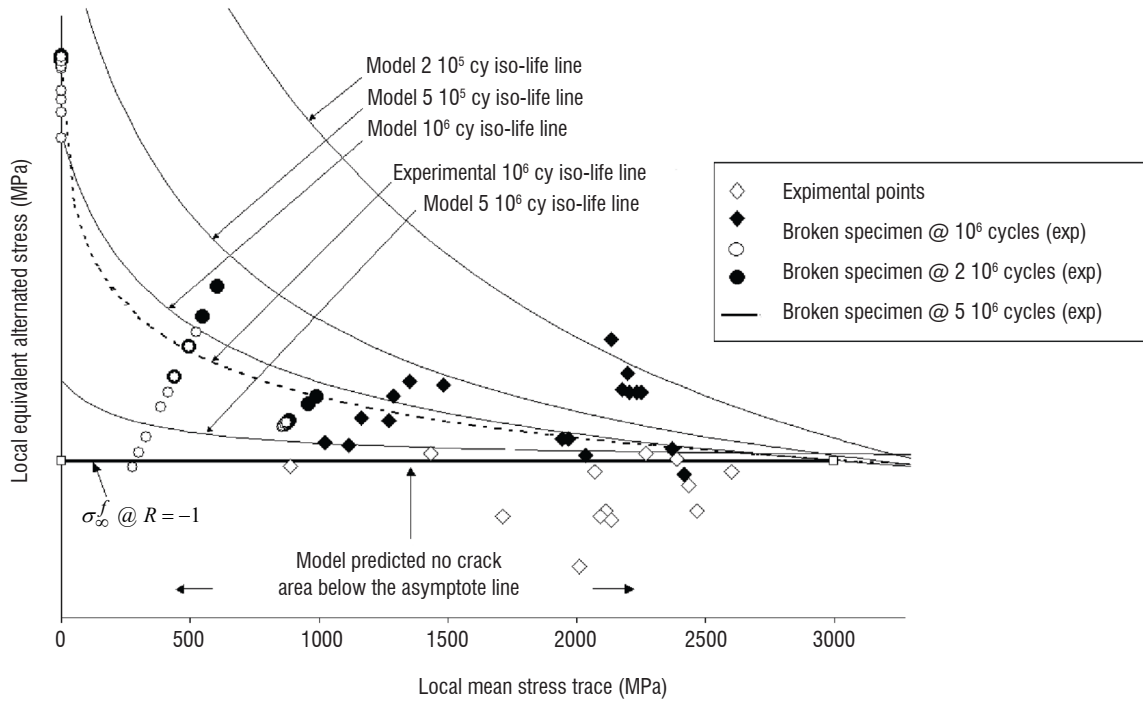


Figure 11 - Multiaxial  $A_{II} / \sigma_f^\infty$  vs.  $\text{tr} \bar{\sigma}$  Haigh diagram (TA6V alloy at a low temperature).

In box 1, from the two-scale damage model constitutive equations, the asymptotic fatigue limit is shown to be linearly mean stress dependent as at infinite lifetime,

$$\text{in 1D: } \sigma_a = \sigma_\ell = \sigma_f^\infty - a \bar{\sigma} \quad (25)$$

$$\text{in 3D, proportional loading: } A_{II} = \sigma_\ell = \sigma_f^\infty - a \text{tr} \bar{\sigma}$$

so that the Sines criterion is retrieved in 3D, under a proportional loading assumption with octahedral stress  $A_{II}$  equal to the Von Mises norm of stress tensor amplitude. The fatigue limit in shear is obtained as  $\tau_f^\infty = \sigma_f^\infty / \sqrt{3}$  for any mean shear stress  $\bar{\tau}$ : it is not mean stress dependent, as experimentally observed [59, 42].

### Bi-linear mean stress effect

A non-linear or at least bilinear modeling of the mean stress effect is sometimes needed if the applications range from alternated fatigue to high mean stress loading [33, 6].

A bilinear mean stress effect on the fatigue asymptote can be introduced into the two-scale damage model, by considering a bilinear definition of the first invariant term of the criterion function at the microscale, as

$$f^\mu = \left( \sigma^\mu - X^\mu \right)_{eq} + K^\mu(\sigma_H) - \sqrt{3} \tau_f^\infty$$

$$K^\mu(\sigma_H) = \begin{cases} 3a_1 \sigma_H & \text{if } \sigma_H \leq \frac{1}{3} \sigma_0 \\ 3a_2 \sigma_H + (a_1 - a_2) \sigma_0 & \text{if } \sigma_H > \frac{1}{3} \sigma_0 \end{cases} \quad (26)$$

where  $a_1$ ,  $a_2$  and the mean stress domain transition stress  $\sigma_0$  are material parameters and  $K^\mu(\sigma_H = 0) = 0$  so  $\tau_f^\infty$  is the fatigue limit mean stress, independent in pure shear.  $K^\mu(\sigma_H) = 3a\sigma_H = a \text{tr} \sigma = a \text{tr} \sigma^\mu$  is recovered and the linear mean stress effect from  $a_1 = a_2 = a$ .

The dependency of the fatigue limit  $\sigma_\ell$  on the mean stress is now obtained as follows. For a positive mean stress:

- for  $\bar{\sigma} \leq \bar{\sigma}_0$   $\sigma_a = \sigma_f^\infty - a_0 \bar{\sigma}$
- for  $\bar{\sigma} > \bar{\sigma}_0$   $\sigma_a = \sqrt{3} \tau_f^\infty - (a_1 - a_2) \sigma_0 - a_2 \bar{\sigma}$

where

$$\sigma_f^\infty = \frac{2\sqrt{3} \tau_f^\infty - (a_1 - a_2) \sigma_0}{2 - (a_1 - a_2)}$$

$$\bar{\sigma}_0 = \frac{\sigma_f^\infty - \sqrt{3} \tau_f^\infty + (a_1 - a_2) \sigma_0}{a_0 - a_2} \quad (27)$$

$$a_0 = \frac{a_1 + a_2}{2 - (a_1 - a_2)}$$

The calculations of an asymptotic multiaxial Haigh diagram (at infinite lifetime) can be found in Appendix A. Note that over the entire range of mean stresses, including the highly negative ones, the Haigh diagram is in fact trilinear.

### Conclusion

The computation of two complementary multiaxial Haigh diagrams has been presented by means of an incremental two-scale damage analysis. Damage and failure are considered as part of the material behavior, in High Cycle Fatigue also, and this even if a structure behaves elastically at the macroscopic scale. The time integration, time step by time step, of the plasticity coupled with the damage microscale constitutive equations determines HCF failure, here the microcrack initiation, simply by the reaching of a critical damage,  $D = D_c$ , in 3D cases, in notch yielding cases, in any general complex fatigue loading cases.

The two scale damage analysis has been carried out on TA6V notched specimens at a low temperature. The TA6V specimens were tested at up to  $10^7$  cycles at different stress ratios, from  $R = 0.5$  up to  $R = 0.9$ . The advantages of notched specimens have been pointed out as twofold,

- on the one hand, they allow an interesting bi-axial stress state to be obtained in the average proportion of 70% in axial and 30% in hoop stresses,
- on the other hand, they allow high stress ratios and high local plastification levels to be easily explored; these levels are often observed in real structures.

This is often not possible with uniaxial (smooth) specimens.

The model has been identified first by fatigue data for a single population of smooth specimens tested at  $R = -1$ . It has then been applied, in a post-processing approach, to notched specimens exhibiting plastification at the notch tip (at different stress ratios  $R$ ). Both the non-rupture events and the numbers of cycles to crack initiation have been correctly predicted. An average factor of 2 has been obtained between

the experimental lifetimes and the computed numbers of cycles to crack initiation (over a 21 notched specimen population).

This work also emphasizes a quite good concordance between the experimental iso-lifetime curves and their theoretical counterparts, at least at  $N_R = 10^6$  for TA6V at a low temperature: they decrease and seem to converge towards a unique asymptote in Haigh diagrams, as the stress ratio increases. This asymptote corresponds to the infinite alternated fatigue limit, a material parameter also called asymptotic fatigue limit, for the considered titanium alloy – a TA6V optimized for aeronautics applications.

The asymptote may not be horizontal, thus leading to a stronger mean stress effect. A way to obtain a linear or piecewise linear Haigh diagram from the two-scale damage model has been finally addressed.

Finally, note that neither the scale nor the gradient effects have been introduced (nor are they needed) in the modeling. A quantitative study of such effects for this titanium alloy is left for further work. It must be noted that the possibilities of gradient modeling within a two-scale damage model can be found, in [16, 46] ■

### Box 1 - Mean stress effect from a two-scale damage model: proof under proportional loading

Under a proportional loading, a time-space multiplicative decomposition can be applied:

$$\sigma = \sigma(t)\Sigma \quad \text{with} \quad \Sigma_{eq} = \sqrt{\frac{2}{3}\Sigma' : \Sigma'} = 1 \quad (1-1)$$

where  $\sigma = \sigma(t) = \text{sign}(\sigma)\sigma_{eq}$  is a scalar function (the signed Von Mises stress) and  $\Sigma$  is a constant tensor, normed, such as  $\text{tr}\Sigma > 0$ , so the stress triaxiality is  $\sigma_H / \sigma_{eq} = \frac{1}{3}\text{sign}(\sigma)\text{tr}\Sigma$ .

At the microscale, due to the Eshelby-Kršner scale transition (5), proportionality is maintained only for deviatoric tensors :

$$\epsilon^{\mu p} = \frac{3}{2}\epsilon^{\mu p}\Sigma' \quad \text{and} \quad X^\mu = X^\mu\Sigma' \quad (1-2)$$

where  $\dot{X}^\mu = C^\mu(1-D)\dot{\epsilon}^{\mu p}$  for the now scalar kinematic hardening law.

The deviatoric part of the scale transition for the deviatoric tensors gives  $\tilde{\sigma}^{\mu'} = \sigma' - 2G(1-\beta)\epsilon^{\mu p} = (\sigma - 3G(1-\beta)\epsilon^{\mu p})\Sigma'$ , so quantities at the microscale can be expressed from the scalar signed Von Mises stress  $\sigma$ :

$$\begin{cases} \text{tr}(\sigma^\mu) = \text{tr}(\sigma) = \sigma\text{tr}(\Sigma) \\ (\sigma^\mu - X^\mu)_{eq} = |\sigma - (3G(1-\beta) + C^\mu)\epsilon^{\mu p}| \end{cases} \quad (1-3)$$

The expression (24), generalized into Eq. (26) for the yield criterion at the microscale, becomes in proportional loading :

$$f^\mu = |\sigma - (3G(1-\beta) + C^\mu)\epsilon^{\mu p}| + K^\mu(\sigma_H) - \sqrt{3}\tau_f^\infty \quad (1-4)$$

The extrema of a cycle at the onset of plasticity  $f = 0$  at both the maximum stress  $\sigma_{Max}$  and minimum stress  $\sigma_{min}$  are

$$\begin{cases} f_{Max} = \sigma_{Max} - (3G(1-\beta)\epsilon^{\mu p} + X^\mu) + K^\mu(\sigma_{HMax}) - \sqrt{3}\tau_f^\infty = 0 \\ f_{min} = -\sigma_{min} + 3G(1-\beta)\epsilon^{\mu p} + X^\mu + K^\mu(\sigma_{Hmin}) - \sqrt{3}\tau_f^\infty = 0 \end{cases} \quad (1-5)$$

Infinite lifetime (endurance) corresponds to a possible pre-yielding, but then to elastic loading at constant  $\varepsilon^{pm}$  and  $X^\mu$  at the microscale, to a stress amplitude lower than  $\sigma_a = \frac{1}{2}(\sigma_{Max} - \sigma_{min}) = \frac{1}{2}(\sigma_{Max}\Sigma' - \sigma_{min}\Sigma')_{eq} = A_{II}$  (due to  $\Sigma_{eq} = 1$ ) determined from both conditions  $f_{Max} = f_{min} = 0$ . In any case, it is  $A_{II} = \sqrt{3}\tau_f^\infty - \frac{1}{2}(K^\mu(\sigma_{Hmin}) + K^\mu(\sigma_{HMax}))$ ,

- if a linear Drucker-Prager expression (24) is used  $\frac{1}{2}(K^\mu(\sigma_{HMax}) + K^\mu(\sigma_{Hmin})) = ktr\bar{\sigma}$  so that linear Sines criterion describing the infinite lifetime domain is obtained :

$$A_{II} = \frac{1}{2}(\sigma_{Max} - \sigma_{min})_{eq} = \sqrt{3}\tau_f^\infty - a tr\bar{\sigma} \quad (1-6)$$

- if a bilinear definition of function  $K^\mu(\sigma_H)$  is used, there are 3 cases :

i)  $tr\sigma_{Max} \leq \sigma_0$  or ii)  $tr\sigma_{min} \geq \sigma_0$  or iii)  $tr(\sigma_{Max}) > \sigma_0$  and  $tr(\sigma_{min}) < \sigma_0$ .

For cases (i) and (ii) the same parameter  $a_i$  acts in  $f_{min}$  and  $f_{max}$  so that the same calculations as previously hold, therefore the mean stress effect is linear (but with different slopes  $a_1$  or  $a_2$ ) as

$$\text{when } tr\sigma_{Max} < \sigma_0 \quad A_{II} = \frac{1}{2}(\sigma_{Max} - \sigma_{min})_{eq} = \sqrt{3}\tau_f^\infty - a_1 tr\bar{\sigma} \quad (1-7)$$

$$\text{when } tr\sigma_{min} > \sigma_0 \quad A_{II} = \frac{1}{2}(\sigma_{Max} - \sigma_{min})_{eq} = \sqrt{3}\tau_f^\infty - (a_1 - a_2)\sigma_0 - a_2 tr\bar{\sigma}$$

In the last case, the two constants  $a_1$  and  $a_2$  act as in eq. (26)

$$\begin{cases} tr\sigma_{Max} > \sigma_0 & f^\mu = \sigma_{Max} - (3G(1-\beta)\varepsilon^{\mu p} + X^\mu) + a_2\sigma_{Max} tr\Sigma + (a_1 - a_2)\sigma_0 - \sqrt{3}\tau_f^\infty = 0 \\ tr\sigma_{min} < \sigma_0 & f^\mu = -\sigma_{min} + 3G(1-\beta)\varepsilon^{\mu p} + X^\mu + a_1\sigma_{min} tr\Sigma - \sqrt{3}\tau_f^\infty = 0 \end{cases} \quad (1-8)$$

By adding the two equations, at identical  $\varepsilon^{pm}$ , the amplitude is obtained:

$$\sigma_a = \sqrt{3}\tau_f^\infty - (a_1 - a_2)\sigma_0 - (a_2\sigma_{Max} + a_1\sigma_{min})tr\Sigma \quad (1-9)$$

Finally, using  $\sigma_{Max} = \bar{\sigma} + \sigma_a$ ,  $\sigma_{min} = \bar{\sigma} - \sigma_a$ ,  $tr\Sigma = tr\sigma / \sigma_{eq}$  and  $\sigma_a = A_{II}$  in such a proportional cyclic loading a linear mean stress effect is obtained, which is stress triaxiality dependent, with a slope in the Haigh diagram different from parameters  $a_1$  and  $a_2$ ,

$$\text{when } \begin{cases} tr\sigma_{Max} > \sigma_0 \\ tr\sigma_{min} < \sigma_0 \end{cases} \quad A_{II} = \frac{2\sqrt{3}\tau_f^\infty - (a_1 - a_2)\sigma_0}{2 - 3(a_1 - a_2)\frac{\sigma_H}{\sigma_{eq}}} - \frac{a_1 + a_2}{2 - 3(a_1 - a_2)\frac{\sigma_H}{\sigma_{eq}}} tr\bar{\sigma} \quad (1-10)$$

In uniaxial tension-compression  $\Sigma = diag[1, 0, 0]$ , there is a diagonal tensor so

$$\sigma_a = \frac{2\sqrt{3}\tau_f^\infty - (a_1 - a_2)\sigma_0}{2 - (a_1 - a_2)} - \frac{a_1 + a_2}{2 - (a_1 - a_2)} \bar{\sigma} = \sigma_f^\infty - a_0 \bar{\sigma} \quad (1-11)$$

This last equation defines the mean stress effect at low mean stress, if a parameter  $\sigma_0$  is identified that is smaller than the uniaxial fatigue limit  $\sigma_f^\infty$ . It thus defines the fatigue limit at zero mean stress  $\sigma_f^\infty$  from the fatigue limit in pure shear  $\tau_f^\infty$  and the parameters  $a_1, a_2, \sigma_0$  of the bilinear  $K^\mu(\sigma_H)$  function.

## Acknowledgements

Snecma and LMT-Cachan would like to especially acknowledge the CNES (Direction des Lanceurs) for its support for this study carried out on the TA6V alloy.

## References

- [1] K. AAS-JACKOBSEN, R. LENSLOW R - *Behavior of Reinforced Columns Subjected to Fatigue Loading*. ACI Journal, 70(3), pp. 199-206, 1973.
- [2] O.H. BASQUIN (1910) - *The Exponential Law of Endurance Tests*. Proc. ASTM, 10, 625–630.
- [3] G. BARBIER, R. DESMORAT, J.P. SERMAGE, A. DUTERTRE, S. COURTIN, J. DEHOUE, D. TCHOU-KIEN - *Mean Stress Effect by Incremental Two Scale Damage Model, LCF6*. 6th International Conference on Low Cycle Fatigue, Berlin, Sept. 8-12, 2008.
- [4] G. BARBIER, R. DESMORAT, B. RAKA - *Mean Stress Effect and Bi-Axial Fatigue of Structures from Two Scale Damage Model*. ICTAM 2008 -22nd International Congress of Theoretical and Applied Mechanics, Adelaide, Australie, August 25-29, 2008.
- [5] A. BENALLAL, R. BILLARDON, I. DOGHRI, L. MORET-BAILLY - *Crack Initiation and Propagation Analyses Taking into Account Initial Strain Hardening and Damage Fields*. Luxmore A. (ed.), Numerical Methods in Fracture Mechanics, Pineridge Press, pp. 337-351, 1987.
- [6] V. BONNAND, J.L. CHABOCHE, P. GOMEZ, P. KANOUTÉ, D. PACOU - *Investigation of Multiaxial Fatigue in the Context of Turboengine Disc Applications*. International Journal of Fatigue 33, 1006–1016, 2011.
- [7] M.W. BROWN, K.J. ILLER - *A Theory for Fatigue Failure under Multiaxial Stress-Strain Conditions* Institution of Mechanical Engineers. Proceedings. vol. 187, no. 65, pp. 745-755. 1973
- [8] J.L. CHABOCHE - *Continuum Damage Mechanics and its Application to Structural Lifetime Predictions*. La Recherche Aérospatiale (English Edition), 4, pp. 37-54, 1987.
- [9] J.L. CHABOCHE - *Development of Continuum Damage Mechanics for Elastic Solids Sustaining Anisotropic and Unilateral Damage*. Int. J. Damage Mechanics, Vol. 2, pp. 311-329, 1993.
- [10] J.L. CHABOCHE, P.M. LESNE - *A Non-Linear Continuous Fatigue Damage Model*. Fatigue Fract Engng Mater Struct 11, 1-17, 1988.
- [11] J.L. CHABOCHE, P.M. LESNE - *Fatigue & Fracture of Engineering Materials & Structures*, 11, p. 1-17, 1988.
- [12] B. CROSSLAND - *Effect of Large Hydrostatic Pressures on the Torsional Fatigue Strength of an Alloy Steel*. Proc. of the Inter. Conf. on fatigue metals Inst. Mech. Engr., pp. 138-149, 1956.
- [13] K. DANG-VAN - *Sur la résistance à la fatigue des métaux*. Sciences et Techniques de l'Armement, vol. 3, pp. 647-722, 1973.
- [14] K. DANG-VAN - *Macro-Micro Approach in High-Cycle Multiaxial Fatigue, Advances in Multiaxial Fatigue*. ASTMSTP1191, D.L. McDowell and R. Ellis Eds., American Society for Testing Materials, Philadelphia, pp. 120-130, 1993.
- [15] R. DESMORAT - *Modélisation et estimation rapide de la plasticité et de l'endommagement*. Habilitation à Diriger des Recherches, Université Paris 6, 2000.
- [16] R. DESMORAT - *Two Scale Damage Model for Fatigue Representation of Gradient Effects*. 6th National Congress on Mechanics, Thessaloniki, Grèce, Vol. 2, p. 318-327, 19-21 July 2001.
- [17] R. DESMORAT, J. LEMAITRE - *Two Scale Damage Model for Quasi-Brittle and Fatigue Damage, Handbook of Materials Behavior Models*. J. Lemaitre Ed., Academic Press, chapter Continuous Damage, Section 6.15, pp. 525-535, 2001.
- [18] R. DESMORAT - *Damage and Fatigue : Continuum Damage Mechanics Modeling for Fatigue of Materials and Structures*. European Journal of Environmental and Civil Engineering (Revue Européenne de Génie Civil), 10, p. 849-877, 2006.
- [19] R. DESMORAT, F. PAUGET, J.P. SERMAGE - *DAMAGE\_2005: a Post-Processor for High Cycle Fatigue under Complex Thermomechanical Loading*. ASME Pressure Vessels and Piping Division Conference, Vancouver, BC, Canada, July 23-27, 2006.
- [20] R. DESMORAT, A. KANE, M. SEYEDI, J.P. SERMAGE - *Two Scale Damage Model and Related Numerical Issues for Thermo-Mechanical High Cycle Fatigue*. Eur. J. Mech A/Solids, Vol. 26, pp. 909-935, 2007.
- [21] R. DESMORAT, F. RAGUENEAU, H. PHAM - *Continuum Damage Mechanics for Hysteresis and Fatigue of Quasi-Brittle Materials and Structures*. International Journal of Numerical and Analytical Methods for Geomaterials, vol. 31, p. 307-329, 2007.
- [22] R. DESMORAT, S. CANTOURNET - *Modeling Micro-Defects Closure Effect with Isotropic/Anisotropic Damage*. International Journal of Damage Mechanics, vol. 17, pp. 65–96, 2008.
- [23] R. DESMORAT, S. OTIN - *Cross-Identification Isotropic/Anisotropic Damage and Application to Anisothermal Structural Failure*. Engineering Fracture Mechanics, 75(11), p. 3446-3463, 2008.
- [24] C. DOUDARD, S. CALLOCH, P. CUGY, A. GALTIER, F. HILD - *A Probabilistic Two Scale Model for High-Cycle Fatigue Life Prediction*, Fatigue Fract. Engng Mater Struct, 28, p. 279-288, 2005.
- [25] J. DUFAILLY, J. LEMAITRE - *Modeling Very Low Cycle Fatigue*. International Journal of Damage Mechanics, 4, p. 153-170, 1995.
- [26] C. ERNY, D. THEVENET, J.Y. COGNARD, M. KÖRNER - *Fatigue Life Prediction of Welded Ship Details*. Marine Structures, 25, p. 13-32, 2012.
- [27] J.D. ESHELBY - *The Determination of the Elastic Field of an Ellipsoidal Inclusion, Related Problems*. Proc. Roy. Soc., London, vol. A241, p. 376, 1957.
- [28] A. FATEMI, L. YANG - *Cumulative Fatigue Damage and Life Prediction Theories: a Survey of the State of the Art for Homogeneous Materials*. International Journal of Fatigue, vol. 20, pp. 9-34, 1998.
- [29] L. FLACELIERE, F. MOREL, A. DRAGON - *Coupling Between Mesoplasticity and Damage in High-Cycle Fatigue*. International Journal of Damage Mechanics, 16, pp. 473-509, 2007.
- [30] D. FRANÇOIS, A. PINEAU, A. ZAOUI - *Comportement mécanique des matériaux – élasticité et plasticité*. Hermès Paris, 1992.
- [31] F. GALLERNEAU, J.L. CHABOCHE - *Fatigue Life Prediction of Single Crystals for Turbine Blade Applications*. International Journal of Damage Mechanics, 8(4), pp. 404-427, 1999.
- [32] A. GANCZARSKI, L. BARWACZ - *Low Cycle Fatigue Based on Unilateral Damage Evolution*. International Journal of Damage Mechanics, 16, pp. 159-177, 2007.

- [33] V. GOMEZ - *Etude en fatigue biaxiale à haute température d'alliages métalliques pour disques de turbomachines aéronautiques*. PhD thesis, Univ. Paul Sabatier, 2001.
- [34] C.T. HUA, D.F. SOCIE - *Fatigue Damage in 1045 Steel under Constant Amplitude Biaxial Loading*. *Fatigue Eng. Mat. Struct.*, 7, 165–179, 1984.
- [35] E. KRÖNER - *On the Plastic Deformation of Polycrystals*. *Acta Metall.*, vol. 9, pp. 155-161, 1961.
- [36] P. LADEVÈZE, J. LEMAITRE, 1984 - *Damage Effective Stress in Quasi unilateral Conditions*. 16th International Congress of Theoretical and Applied Mechanics, Lyngby, Denmark.
- [37] D.B. LANNING, T. NICHOLAS, G.K. HARITOS - *On the use of Critical Distance Theories for the Prediction of the High Cycle Fatigue Limit Stress in Notched Ti-6Al-4V*. *International Journal of Fatigue*, vol. 27, pp. 45-57, 2005.
- [38] N. LAUTROU, D. THEVENET, J.Y. COGNARD - *A Fatigue Crack Initiation Approach for Naval Welded Joints*. *Oceans 2005 - Europe*, 2, p. 1163 - 1170, 2005
- [39] H.H.E. LEIHZOLZ - *On the Modified S-N Curve for Metal Fatigue Prediction and its Experimental Verification*. *Engineering Fracture Mechanics*, vol. 23, pp. 495-505, 1986.
- [40] J. LEMAITRE, J.L. CHABOCHE - *A Non-Linear Model of Creep-Fatigue Damage Cumulation and Interaction*. Symposium IUTAM, Gothenburg, 2-6 september 1974.
- [41] J. LEMAITRE, A. PLUMTREE - *Application of Damage Concepts to Predict Creep-Fatigue Failures*. *Journal of Engineering Materials Technology*, vol. 101, pp. 284–292, 1979.
- [42] J. LEMAITRE, J.L. CHABOCHE - *Mécanique des matériaux solides*. Dunod 1985, *Mechanics of solid materials (3rd Edition 2009)*, Oxford University Press, 1991 (english translation).
- [43] J. LEMAITRE - *A course on Damage Mechanics*. Springer Verlag, 1992.
- [44] J. LEMAITRE, I. DOGHRI - *Damage 90: a Post-Processor for Crack Initiation*. *Comp. Methods Appl. Mech. Engrg.* 115: 197-232, 1994.
- [45] J. LEMAITRE, J.P. SERMAGE, R. DESMORAT - *A two Scale Damage Concept Applied to Fatigue*. *International Journal of Fracture*, vol. 97, pp. 67-81, 1999.
- [46] J. LEMAITRE, R. DESMORAT - *Engineering Damage Mechanics : Ductile, Creep, Fatigue and Brittle Failures*. Springer, 2005.
- [47] Z.X. Li, F.F. Jiang, Y.Q. Tang - *Multi-Scale Analyses on Seismic Damage and Progressive Failure of Steel Structures*. *Finite Elements in Analysis and Design*, 48, p. 1358-1369, 2012.
- [48] D.L. MCDOWELL - *Damage Mechanics and Metal Fatigue: A Discriminating Perspective*. *International Journal of Damage Mechanics*, 8, pp. 376-403, 1999.
- [49] S.S. Manson, M.H. Hirschberg 1964 - *Fatigue: An Interdisciplinary Approach*. Syracuse University Press, Syracuse, N.Y.
- [50] A. MARMI, A. HABRAKEN, L. DUCHENE - *Multiaxial Fatigue Damage Modelling at Macro Scale of Ti6AL4V Alloy*. *International Journal of Fatigue*, 31, 2031-2040, 2009.
- [51] V. MONCHIET, E. CHARKALUK, D. KONDO - *Plasticity-Damage Based Micromechanical Modelling in High Cycle Fatigue*. *C. R. Mecanique*, 334, p. 129-136, 2006.
- [52] F. MOREL - *A Critical Plane Approach for Life Prediction of High Cycle Fatigue under Multiaxial Variable Amplitude Loading*. *International Journal of Fatigue* vol. 22(2), pp. 101-119, 2000.
- [53] T. NICHOLAS - *Critical Issues in High Cycle Fatigue*. *International Journal of Fatigue*, 21(1), pp. 221-231, 1999.
- [54] M.H. PAAS, P.J.G. SCHREURS, W.A.M. BREKELMANS - *A Continuum Approach to Brittle and Fatigue Damage: Theory and Numerical Procedures*. *Int. J. Solids Struct.*, 30, 579–599, 1993.
- [55] I.V. PAPADOPOULOS - *A High-Cycle Fatigue Criterion Applied in Biaxial and Triaxial Out-of-Phase Stress Conditions*. *Fatigue & Fracture of Engineering Materials & Structures* vol. 18(1), pp. 79-91, 1995.
- [56] I.V. PAPADOPOULOS, P. DAVOLI, C. GORLA, M. FILIPPINI, A. BERNASCONI - *A Comparative Study of Multiaxial High-Cycle Fatigue Criteria for Metals*. *International Journal of Fatigue* Vol. 19(3), pp. 219-235, 1997.
- [57] J.P. SERMAGE, J. LEMAITRE, R. DESMORAT - *Multiaxial Creep Fatigue under Anisothermal Conditions*. *Fatigue and Fracture of Engng Mater. & Struct.*, 23(3), pp. 241 - 252, 2000.
- [58] M. SAUZAY - *Effet de surface en fatigue polycyclique*. PhD thesis Univ. Paris 6, 2000.
- [59] G. SINES - *Behavior of Metals under Complex Static and Alternating Stresses*. In: Sines, G., Waisman, J.L. (Eds.). McGraw-Hill, New York, pp. 145–169, 1959.
- [60] R. SMITH, P. WATSON, T. TOPPER - *A Stress-Strain Function for the Fatigue of Metals*. *Journal of Mat.*, vol. 5, pp. 767-778, 1970.
- [61] K. THEPVONGSA, Y. SONODA, H. HIKISAKA - *Journal of Applied Mechanics*, 6, p. 1227-1234, 2003.

## AUTHORS



**Rodrigue Desmorat.** A former student of the Ecole Normale Supérieure de Cachan (ENSC) and Research Associate in Mechanics, Rodrigue Desmorat, 47, has been an Assistant Professor at the University Paris 6. Since 2002, he has been a full Professor at ENSC and carries out research at the LMT-Cachan in the field of Damage Mechanics. He is the co-author of two books.



**Pierre Gaborit.** A graduate from Arts et Métiers ParisTech and Karlsruher Institut für Technologie in Mechanical Engineering, Pierre Gaborit, 27, carried out his PhD research at the LMT-Cachan (Ecole Normale Supérieure de Cachan). This work will be defended in the second half of 2015. Since July 2014 he has been working as a Material Engineer for forged products at Snecma.



**Alban du Tertre.** A graduate from the ECAM Lyon, Alban du Tertre, 40, joined the Space Engine Division of Snecma at Vernon (F) in 1999. He was successively in charge of thermomechanical computations and of powder metallurgy component development in the cryogenic turbo-pump department. He then managed various research and methodological projects, mainly linked to HCF and LCF fatigue applied to rocket engine components, in cooperation with the LMT Cachan, ONERA, the Pprime Institute, etc. Promoted to Expert status in 2014, he now works as a mechanical development project manager in the combustion device design office.